A Quaternion Weighted Fourier Linear Combiner for Modeling Physiological Tremor

Kabita Adhikari, *Student Member, IEEE*, Sivanagaraja Tatinati, *Member, IEEE*, Wei Tech Ang, *Member, IEEE*, Kalyana C. Veluvolu, *Senior Member, IEEE*, and Kianoush Nazarpour*, *Senior Member, IEEE*

***Abstract*—Goal: The present work offers a new approach to model physiological tremor aiming at attenuating undesired vibrations of the tip of microsurgical instruments. Method: Several tremor modeling algorithms, such as the weighted Fourier linear combiner (wFLC), have proved effective. They however treat the 3-dimensional (3-D) tremor signal as three independent 1-D signals in the x, y, and z axes. In addition, the force f by which a surgeon holds the instrument has never been taken into account in modeling. Hence conventional algorithms are inherently blind to any potential multi-dimensional couplings. Results: We first show that there exists statistically-significant subject- and task-dependent coherence between data in the x, y, z, and f axes. We hypothesize that a filter that models the tremor in 4-D (x, y, z, and f) yields a more accurate model of tremor. We therefore developed a quaternion version of the wFLC algorithm and termed it QwFLC. We tested the proposed QwFLC algorithm with real physiological tremor data that was recorded from five novice subjects and four experienced microsurgeons. Although compared to wFLC, QwFLC requires 6 times larger computational resources, we showed that QwFLC can improve the modeling by up to 67% and that the improvement is proportional to the total coherence between the tremor in xyz and the force signal. Conclusions: Taking into account the interactions of 3-D tremor data and the force enhances the modelling performance significantly. Significance: With more accurate physiological tremor modeling, enhanced tremor cancellation performance in microsurgery may be achieved.**

***Index Terms*—Physiological tremor, quaternion algebra, weighted Fourier linear combiner**

I. Introduction

TREMOR is an unintentional oscillatory movement of the body parts presented mainly in the hands. The tremor is broadly classified into two categories: pathological and physiological [1], [2]. Pathological tremor is one of the most extreme forms of movement disorders. Physiological tremor however is not a movement disorder and it can be observed in every normal individual. The amplitude of the physiological tremor ranges typically from $50-100\mu$m in each of the xyz axes (Figure 1) [3], [4]. The spectrum of the physiological tremor can display multiple dominant peaks spread between 6Hz and 14Hz [3], [5]–[7].

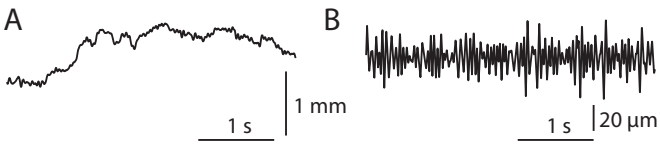

Fig. 1. A representative trace of the recorded position of the tip of an instrumented stylus in the x axis during a task (A); and the physiological tremor extracted by bandpass filtering between 5Hz and 20Hz in (B).

With the advancement in medical technologies, robotic assisted surgery evolved to achieve minimally invasive surgery and enhance surgical dexterity. Since the creation of first laparoscopic tool in 1985 [8], robotic arms have improved dramatically. Systems such as LARS [9], ZEUS [10] and Da Vinci [11] provide several movement degree of freedom with capability to mimic natural wrist and hand motions. The "Steady Hand Robot" system [12] was designed to be simultaneously held by both surgeon and an actively controlled robotic arm which controls the force exerted by the surgeon to provide smooth, tremor free precise manipulation. In addition, there has been a rise of smart surgical hand-held devices to perform sub-millimetre manipulations. For instance, the "Micron" system proposed by Riviere [13] offered more flexibility and 3-D micromanipulation. Recently Gonenc et. al. [14] have shown that Steady Hand Robot and Micron can provide similar improvements in terms of tremor compensation in microsurgeries.

Physiological tremor, although not so much of a problem in day-to-day life, can lead to substantial imprecisions in microsurgery in which a positioning accuracy of $10-20\mu$m is typically required [1], [3], [15]. Natural upper-limb movement is often a combination of regular sub-movements between 1Hz and 4Hz [16], [17]. Therefore physiological tremor can be filtered out readily with linear low-pass filters. However, to achieve sharp cut-offs, linear filters need a large number of taps. Consequently they lead to considerable time delays [18]. Therefore, they are not used in microsurgery in which real-time filtering is required [3]. Moreover, factors such as anxiety and fatigue can modulate the magnitude and the spectrum

Manuscript received August 03, 2015. The work of K. Adhikari is supported by Newcastle University. K. C. Veluvolu is supported by the Basic Science Research Program, National Research Foundation of Korea (NRF), Ministry of Education, Science and Technology (2014R1A1A2A10056145). The work of K. Nazarpour is supported by EPSRC (EP/M025977/1 and EP/M025594/1).

A MATLAB implementation of the QwFLC algorithm supporting this publication is openly available under an "Open Data Commons Open Database License". Additional metadata are available at: 10.17634/137930-1. Please contact Newcastle Research Data Service at rdm@ncl.ac.uk for access instructions.

K. Adhikari is with the School of Electrical and Electronic Engineering, Newcastle University, UK (E-mail: Kabita.Adhikari@Newcastle.ac.uk).

K. C. Veluvolu is with the School of Electronics Engineering, College of IT Engineering, Kyungpook National University, Daegu, South Korea.

W. T. Ang is with School of Mechanical and Aerospace Engineering, Nanyang Technological University, Singapore.

*K. Nazarpour is with the School of Electrical and Electronic Engineering and the Institute of Neuroscience, Newcastle University, Newcastle NE1 7RU, UK (correspondence e-mail: Kianoush.Nazarpour@Newcastle.ac.uk).

of the physiological tremor significantly [2]. Such dynamics render fixed linear filters ineffective.

Riviere and Thakor [3] proposed adaptive filtering for tremor cancellation in microsurgery. In this scheme to attenuate the tremor at the tip of a hand-held instrument adaptively, a signal analysis unit models the tremor and actuates the tip of the instrument with an anti-phase signal with minimal delay. They used a least mean square (LMS)-based adaptive filtering algorithm for modeling. Others followed a similar process to model or predict non-stationary amplitude and frequency of tremor [5], [7], [15].

Tremor modeling using adaptive filters typically require a reference signal that is highly correlated with the tremor signal. The amplitude of typical physiological tremor is however approximately 50 times smaller than that of the voluntary motion. This mismatch can push the adaptation towards the dominant components of the voluntary movement rather than that of the tremor [19]. Hence, the tremor signal is extracted in real-time using digital filters prior to adaptive modeling [5], [7], [15]. Building upon the Fourier linear combiner (FLC) structure proposed in [20], Riviere and Thakor [3] modeled the tremor signal with a truncated Fourier series representation in which the dominant tremor frequency was tracked by maintaining a running sum of the all preceeding frequency updates. The resultant sum modulated a bank of sine and cosine bases and their harmonics. These bases were scaled then by a second set of weights to track the amplitude of the tremor signal. This algorithm was called weighted Fourier linear combiner (wFLC) and it has been tested widely in different settings and extended to other applications modeling of gait [21] or analysis of atological tremor [22]. The proposed QwFLC filter will still need the reference tremor signal extracted offline from a mixture of voluntary and tremulous movement.

The wFLC algorithm and all its extensions treat the 3-D (x, y, and z) tremor signal as three independent 1-D signals. In addition, no previous studies have tested whether inclusion of the force f by which a surgeon holds an instrument improves the modeling accuracy. We therefore hypothesized that an adaptive system which incorporates any multi-dimensional couplings can improve the tremor modeling performance.

Quaternion algebra can preserve natural representation of 3-D or 4-D processes. Due to such advantages quaternion operation has been popular in many areas, e.g. image processing [23] and wind modeling [24]. A quaternion LMS (QLMS) was recently developed in [25]. QLMS incorporates both the covariance and the pseudo-covariance of the input 4-D signals to update the new filter parameters to improve signal modeling or prediction [25].

In Section II we extend the conventional FLC and wFLC algorithms to their quaternion versions, that is, QFLC and QwFLC. We then evaluate their performance with synthetic and real data in Section III. Section IV and V are our Discussions and Conclusions, respectively. Preliminary results of this work were reported in [26], [27].

II. Methods

A. Experimental Setup

Participants: Five medical students with basic surgical skills (novice group) and four experienced microsurgeons (surgeon group) took part in this study. All subjects gave their informed written consent before participation. The study was approved by the local ethics committee at Nanyang Technological University [28].

Measurement: With the motivation to develop smart hand-held surgical instrument capable of tracking and cancelling tremor during microsurgery, the optical micro motion sensing system (M^2S^2) was developed in [29]. The system was designed to track the 3-D displacement of the tip of a microsurgical instrument in a laboratory suite, while the subjects carried out some realistic task similar to the micro-manipulation performed during real microsurgeries [29], [30].

M^2S^2 has an embedded microsensing system with two orthogonally-placed position sensitive detectors to track the 3-D displacement of the tip of a microsurgical instrument in real-time. The *workspace* is a target platform of dimension $10 \times 10 \times 10\text{mm}^3$ where tasks are performed. An IR diode illuminates the workspace and the 3-D displacement of a small white ball, that is placed at the tip of the stylus, is calculated by the centroid position of the reflected infra-red rays onto the detectors. For visual feedback a $19''$ flat LCD TV monitor is used which was placed 70cm away from the subjects.

Subjects were asked to seat facing the monitor and to hold an instrumented stylus between their index and thumb fingers with the wrist relaxed on an armchair and elbow held at 90 degrees. The stylus has similar mass characteristics to those of typical surgical forceps.

A force sensor (FSG15N1A, Honeywell Sensing and Control, USA) is mounted on the stylus to measure the grip force (range: $0 - 15$N). The position and force data are digitized at 250 samples per second with a data acquisition card (PD-MF-16-150, United Electronic Industries, USA) with a 16 bits resolution. For further details, the reader is referred to [28]–[30].

To generate an appropriate reference signal for our adaptive algorithms, we pre-filtered (offline) the recorded position and force data in each axis independently with a zero-lag 5th-order Butterworth digital filter with a passband of $5 - 20$Hz.

Tasks: Subjects performed two tasks:

- *Pointing*: Two dots were displayed on the monitor screen. One was a fixed white dot and another an orange dot which moved according to the tool tip position held by the subjects. The subjects were asked to overlap the orange dot with the white dot and to maintain the same position for 30s [28];
- *Tracing*: Subjects were asked to trace the circumference of a white circle (diameter: 4mm) which was shown on the screen. A dot was used as cursor for the subjects to move along the circle clockwise as accurately as possible with the speed which was realistic to surgical manipulation as the subjects had surgical knowledge [28]. The tracing task was carried out on the $x - y$ horizontal plane. The total tracing time for each subject was 30s.

Average tracing speeds were 1.59mms^{-1} and 1.96mms^{-1} for novice and surgeon subjects, respectively. This speed did not vary significantly among subjects.

Data were shortened to 28s to counter the transient effect of filtering. Some subjects performed the two tasks under three different visual magnification conditions: ×1, ×2 and ×10. Here, we used data from the ×1 magnification condition in which data from all subjects are available.

B. Time- and Frequency-Domain Correlation Analysis

To investigate force and tremor dependency, we first performed a simple time-domain correlation analysis. Time-domain correlation R between x, y, z, and f were calculated, for instance $R_{xy}(l) = \sum_{n=-\infty}^{\infty} x(n)y(n-l)$ where l denotes the time-lag. Time-domain correlation analysis can reveal broadband and strong correlations readily. To identify the associations when signals have moderate but frequency-specific correlation, frequency-domain techniques, such as coherence analysis, may be more effective [31], [32]. Coherence offers a bounded measure and reflects linear interaction between two processes, with 0 and 1 occurring in case of no and perfect linear dependency, respectively [33]. Coherence (Coh) between all pair of x, y, z and f were calculated, for example coherence between x and y (denoted by Coh_{xy}) is calculated as

$$\text{Coh}_{xy}(fr) = \frac{|\text{PSD}_{xy}(fr)|^2}{\text{PSD}_{xx}(fr)\text{PSD}_{yy}(fr)} \tag{1}$$

where fr is the frequency, and PSD_{xx} and PSD_{xy} denote the power spectral density of x and the cross-spectral density between x and y, respectively. In calculating the PSDs, a standard Hanning window (width, 1s) was used.

Following the approach adopted in [32]–[34], each data file was split into $D = 28$ non-overlapping 1s segments. The statistical significance threshold value for the estimated coherence spectra was calculated under the hypothesis of independence with $s = 1 - \alpha^{1/(D-1)}$. Coherence values larger than s were considered significantly different from zero with p-values smaller than $\alpha = 0.05$ [33].

Coherence analysis could show statistically significant but artificial coherence when the PSD magnitude of one or both of the signals is very small. In order to avoid such a problem, we first analyzed the PSD of all signals in the $5-15$Hz frequency range. We ensured that coherence values are only accepted if the signal power is within the 3dB range of the peak power in each axis. The PSD analysis was carried out for all subjects, all four axes and in both tasks. We chose first to estimate coherence between the data in the x, y, and z axes. We then repeated this analysis between data in the x, y, and z axes and the f data.

C. Algorithm Development

Here, we briefly review the FLC and wFLC algorithms that are both based on the LMS algorithm. We then describe the proposed QFLC and QwFLC structures.

1) Fourier Linear Combiner: Any periodic or quasi-periodic signal s of a *known* main frequency ω_0 can be estimated adaptively as $\hat{s}$ by combining sine and cosine bases [20]:

$$\begin{aligned} n_{h,t} &= \begin{cases} \sin(h\omega_0 t) & 1 \le h \le H \\ \cos[(h-H)\omega_0 t] & H+1 \le h \le 2H \end{cases} \\ \hat{s}_t &= \mathbf{w}_t^T \mathbf{n}_t \end{aligned} \tag{2}$$

where $\mathbf{w}_t = [w_{1,t}, w_{2,t}, \cdots, w_{2H,t}]^T$ is a vector of the adaptively calculated Fourier series coefficients, $\mathbf{n}_t = [n_{1,t}, n_{2,t}, \cdots, n_{2H,t}]^T$, t denotes the time, H is the number of harmonics in the model representing the measured signal s and $\{.\}^T$ denotes the vector transpose operation.

The unknown amplitude of the signal is then tracked using the adaptation law $\mathbf{w}_{t+1} = \mathbf{w}_t + \mu e_t \mathbf{n}_t$ with e_t being the error and calculated as $e_t = s_t - \hat{s}_t = s_t - \mathbf{w}_t^T \mathbf{n}_t$. The parameter μ is a learning rate governing the speed of adaptation to the changing amplitude of the signal. Whilst this algorithm serves as the basis for the methods developed in the following, it is not directly applicable in tremor modeling because physiological tremor has multiple unknown peaks in the frequency range of $6-14$Hz [35], [36].

2) Weighted Fourier Linear Combiner: The wFLC algorithm is a frequency weighted version of FLC [3]. It can track multiple tremor frequencies by modeling them as a running sum of an initial reference frequency and replacing the fixed ω_0 with its time-varying version $\omega_{0,k}$. The formulae for frequency update in wFLC are [3]:

$$m_{h,t} = \begin{cases} \sin(h\sum_{k=0}^{t}\omega_{0,k}) & 1 \le h \le H \\ \cos\left[(h-H)\sum_{k=0}^{t}\omega_{0,k}\right] & H+1 \le h \le 2H \end{cases} \tag{3}$$

$$\omega_{0,t+1} = \omega_{0,t} + \mu_\omega e_t \sum_{h=1}^{H} h(w_{h,t}m_{h+H,t} - w_{h+H,t}m_{h,t}), \tag{4}$$

where $m_{h,t}$ is the h-th element of the vector $\mathbf{m}_t$. The tremor amplitude is then tracked with the adaptive weights $\mathbf{w}_{t+1} = \mathbf{w}_t + \mu_\mathbf{w} e_t \mathbf{m}_t$ with adaptation error $e_t = s_t - \hat{s}_t = s_t - \mathbf{w}_t^T \mathbf{m}_t$. Learning rates μ_ω and $\mu_\mathbf{w}$ govern the step size of the frequency and the amplitude updates.

Conventionally, with wFLC, the tremor in the x, y, and z dimensions are modeled independently. To account for the couplings, we propose the use of quaternion algebra. A brief review of quaternion algebra is presented in Appendix A.

D. Quaternion Fourier Linear Combiner

We extended the FLC into its quaternion version (QFLC) by utilizing the quaternion LMS (QLMS) formalism proposed in [25]. Figure 2 depicts a block diagram of the proposed structure. In this structure $\mathcal{S}_t$ is the quaternion variable whose real component is the recorded force $s_{f,t}$ and its imaginary components are the tremor recorded in each axis, $s_{x,t}$, $s_{y,t}$, and $s_{z,t}$ at time t, that is, $\mathcal{S}_t = s_{f,t} + s_{x,t}i + s_{y,t}j + s_{z,t}k$

With QFLC, we can model the amplitude of a 4-D process of a known fundamental frequency Ω_0 with harmonics $h = 1, \cdots, H$. Each harmonic forms a quaternion vector. Consequently, vectors $\mathbf{w}_t$ and $\mathbf{n}_t$ in FLC, are transformed to their quaternion versions $\mathcal{W}_t$ and $\mathcal{N}_t$, respectively. Therefore for each harmonic h:

$$\mathcal{W}_{h,t} = w_{f,h,t} + w_{x,h,t}i + w_{y,h,t}j + w_{z,h,t}k. \tag{5}$$

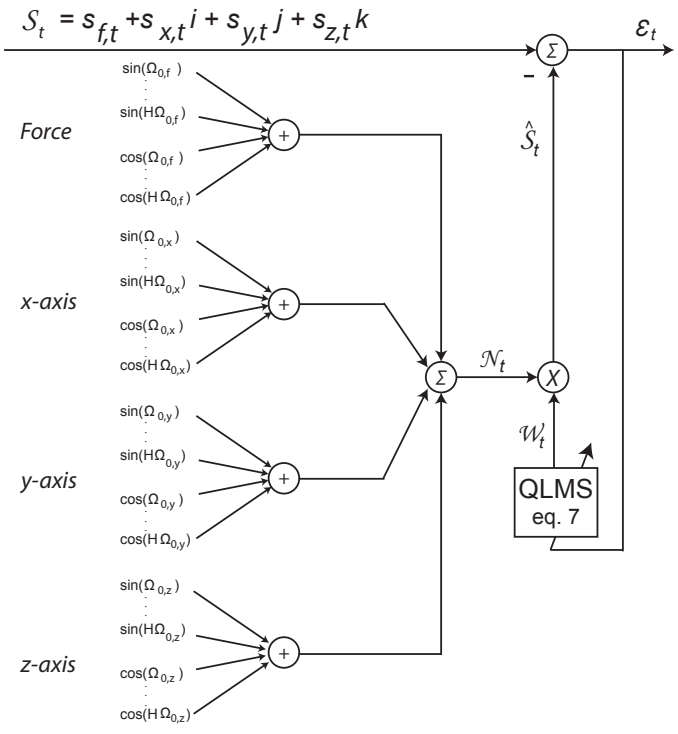

Fig. 2. A block diagram for the QFLC algorithm. Symbols Σ and X represent quaternion summation and multiplication, respectively.

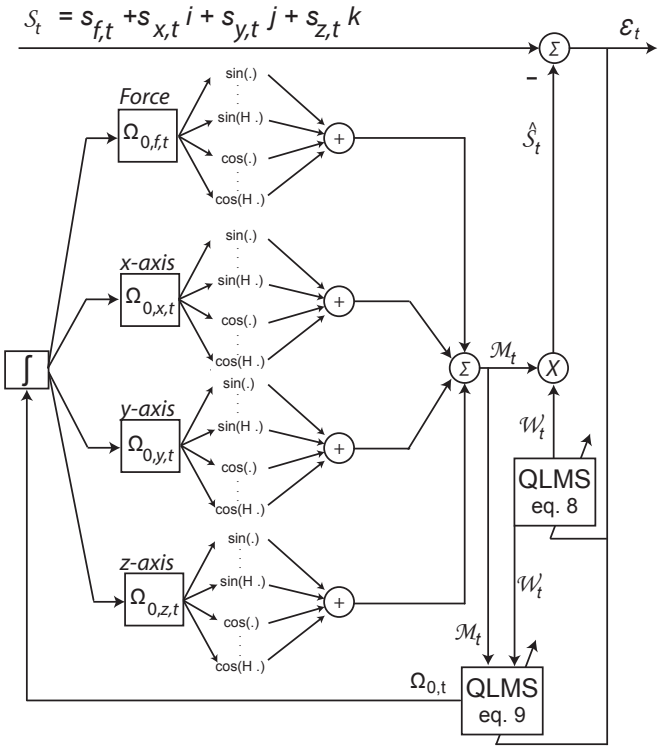

Fig. 3. A block diagram for the QwFLC algorithm. Symbol $\int$ denotes the integration operation.

Following the standard LMS formulation, the quaternion adaptation error is calculated with

$$\mathcal{E}_t = \mathcal{S}_t - \hat{\mathcal{S}}_t = \mathcal{S}_t - \mathcal{W}_t^T \mathcal{N}_t, \tag{6}$$

where $\hat{\mathcal{S}}_t$ denotes an approximation of $\mathcal{S}_t$. Finally, the weight update equation follows the standard QLMS algorithm [25]:

$$\mathcal{W}_{t+1} = \mathcal{W}_t + \mu_{\mathcal{W}}(2\mathcal{E}_t \mathcal{N}_t^* - \mathcal{N}_t^* \mathcal{E}_t^*), \tag{7}$$

where $\mu_{\mathcal{W}}$ is the learning rate which determines speed of convergence and $\{.\}^*$ denotes the quaternion conjugate transpose operation.

Note that in equation (7), $\mathcal{W}_t$ includes the weights for all H harmonics. In addition, it is straightforward to expand QFLC to have axis-specific learning rates.

To measure the efficiency of the QFLC algorithm, we simulated a 3-D reaching task. The hand velocity was modeled with a half-sine wave with a maximum velocity 350mms^{-1}. The instantaneous hand position was then calculated by integrating the velocity profile. QFLC, much like FLC, can track only one frequency. Hence the same 10Hz signal was added to the signals in all 3-D axes to represent the tremor. Note that, in a real-life case, the tremor spectrum in the three dimensions can be different. In addition, independently-generated Gaussian noise was added to data in *xyz*. Simulation was performed with noise levels from -15dB to 15dB (interval 5dB) signal-to-noise (SNR) levels. At each SNR level we repeated the simulations 10 times. In the first iteration we initialised the filter weights $\mathcal{W}$ randomly and independently across *xyz* axes. To achieve a fair comparison, the same initialization $\mathbf{w}$ and $\mathcal{W}$ values were used in the following repetitions. Finally to compare adaptation speed of the QFLC and the FLC algorithms, we calculated the time-lag of the peak cross-correlation function between the original and the modelled 10 Hz signals in consecutive non-overlapping 1s windows.

Since there was only one frequency to track, we fixed the number of harmonics H to 1. This made the filter length ($L = 2H + 1 = 3$). To have a fair comparision, the learning rate for both algorithms was $\mu = 7 \times 10^{-4}$. This learning rate was chosen empirically to optimize the error and convergence rate. To provide enough time for settlement, the simulation was run for $20s$.

E. Quaternion Weighted Fourier Linear Combiner

Despite straightforward development, QFLC is not applicable in real-life tremor modeling since the tremor frequency Ω_0 is neither known nor constant. Therefore, we developed a frequency weighted version of QFLC and called it QwFLC. Figure 3 depicts the block diagram of the proposed QwFLC in which the two quaternions $\mathcal{W}_t$ and $\Omega_{0,t}$ are updated using two separate QLMS blocks to track the amplitude and the frequency of the 4-D tremor signal. Similar to equation (7), the update equation for $\mathcal{W}$ is

$$\mathcal{W}_{t+1} = \mathcal{W}_t + \mu_{\mathcal{W}}(2\mathcal{E}_t \mathcal{M}_t^* - \mathcal{M}_t^* \mathcal{E}_t^*) \tag{8}$$

where $\mathcal{M}_t$ is the quaternion version of $\mathbf{m}_t$ defined earlier in the derivation of wFLC. The frequency update equation in the quaternion domain will then be

$$\Omega_{0,t+1} = \Omega_{0,t} + \mu_{\Omega}(2\mathcal{E}_t \mathcal{G}^* - \mathcal{G}^* \mathcal{E}_t^*), \tag{9}$$

where $\mathcal{G}$ is

$$\mathcal{G} = \sum_{h=1}^{H} h(\mathcal{W}_{h,t}\mathcal{M}_{h+H,t} - \mathcal{W}_{h+H,t}\mathcal{M}_{h,t}). \quad (10)$$

Finally, adaptation error is calculated as $\mathcal{E}_t = \mathcal{S}_t - \hat{\mathcal{S}}_t = \mathcal{S}_t - \mathcal{W}_t^T \mathcal{M}_t$. Similar to QFLC, we kept the learning rates $\mu_{\mathcal{W}}$ and μ_Ω fixed across all axes.

For QwFLC, two cases were considered. In case 1, the data recorded by the force sensor was not included in $\mathcal{S}_t$ and hence the quaternion was purely imaginary comprising only the position information in the x, y, and z dimensions. We denote this case with QwFLC-3D. In the second case, the force data was included in the quaternion $\mathcal{S}_t$ as its real part in addition to position information in the x, y, and z dimensions. The algorithm developed for this case is referred to as QwFLC-4D. In order to provide a fair comparison of performance between WFLC and the proposed methods, we chose the wFLC and QwFLC parameter values empirically to best fit both algorithms. To observe the effect of variability of the parameters we have varied the frequency learning rate μ_Ω between 7×10^{-5} to 9×10^{-5} (resolution 2×10^{-6}) and the amplitude learning rate $\mu_{\mathcal{W}}$ between 0.07 to 0.08 (resolution 0.001). Increasing these learning rates further can shorten the transition time slightly however could result in instability. The standard values of $M = 1$, $\mathbf{w} = \mathbf{0}$, and $\mathcal{W} = \mathbf{0}$ were chosen and the initial frequency value was set to 0.1508 (6Hz). We fixed the number of harmonics H to 1 and hence the filter length was $L = 2H + 1 = 3$.

F. Performance Indices

To quantify the modeling performance of all algorithms we used two performance indices:

1) Root-mean square error (RMSE): Where $\mathcal{X}_{org,i}$ and $\mathcal{X}_{mod,i}$ represent the i-th sample of the observed and modeled quaternion signals and K denotes their length, the RMSE index is defined as

$$RMSE = \sqrt{\frac{\sum_{i=1}^{K}(\mathcal{X}_{org,i} - \mathcal{X}_{mod,i})^2}{K}}. \quad (11)$$

In the case of perfect reconstruction, RMSE will be zero. Therefore the lower the RMSE, the better the modeling.

2) Time delay: In an ideal adaptive modeling system, the time delay between the original and modeled signal is zero. As a second measure of performance, therefore, we calculated the cross-correlation between 100 randomly-selected 5s long segments of the $\mathcal{X}_{org}$ and the $\mathcal{X}_{mod}$ signals in each axis. This was repeated in all subjects, for both tasks and the three algorithms: wFLC, QwFLC-3D, and QwFLC-4D. For each data segment, we registered the time-lag index of the cross-correlation function peak (argument of maximum cross-correlation):

$$\tau_{delay} = \arg\max\{(\mathcal{X}_{org} \star \mathcal{X}_{mod})(t)\} \quad (12)$$

where $\star$ denotes the cross-correlation operation.

Finally, for comparison purposes, we normalised the counts of 0, 1, or 2 time-lags to the total number of cross-correlations function that we computed across both subject groups and both tasks for all algorithms.

G. Computational Complexity

To realise the suitability of the proposed algorithm in real-time applications, we have compared computational complexity of FLC, QFLC, wFLC, and QwFLC. The complexity is measured by calculating the total number of multiplications and additions required per input data while executing the algorithm. The running time complexity is also expressed in $O(.)$ notation to express rate of growth of computational time in terms of order of the filter length. A full description of the derivation of the computational complexity is provided in the Supplementary Material.

III. Results

A. Correlation Analysis Results

With a standard correlation analysis, we found that the tremor components in the x, y, and z dimensions are not independent time series and there exists a subject-specific and task-specific coupling between axes. As an example, Figure 4 (A.1 and B.1) shows strong correlations in the xyz axes for a surgeon carrying out the two tasks. However, in the time-domain correlation between xyz and f plots, it is very difficult to observe any clear correlation structure. We tested the hypothesis that moderate narrowband correlations between tremor in the xyz axes and force f signal cannot be detected if the $5-20$Hz band is considered. We therefore used the coherence analysis to examine correlations in the frequency domain.

Before we proceed with the coherence analysis, with the PSD analysis, we found that the tremor power was distributed in the frequency range of $5-15$Hz for most subjects. Analysing the PSDs in all subjects for both tasks, we identified the lowest peak power as $5\times10^{-12}\mu m^2/Hz$ for the tracing task, and took our reference power level as its half power point (-3dB: $3.5\times10^{-12}\mu m^2/Hz$). For the pointing task we found the lowest peak power of $4\times10^{-12}\mu m^2/Hz$, and took our reference power level (-3dB: $2.8\times10^{-12}\mu m^2/Hz$). Gray boxes in Figure 4 (A.2 and B.2) show the selected power spectral densities above the calculated reference levels for a surgeon subject in the xyz tremor axes and for the force signal.

We further evaluated the calculated coherence values with a significant threshold at $s = 0.1$ as explained earlier. The top three plots in Figure 4 (A.3 and B.3) show coherence estimates for the same surgeon subject with the dashed line signifying the threshold coherence. Note that in Figure 4 (A.3 and B.3), there are peaks above the threshold where the signal power is minimal, for an example in Figure 4 A.3 Coh_{xy} has coherence value above the threshold between $4-12$Hz and there is another peak at 17Hz. However PSD_{xx} and PSD_{yy} are only substancial in the ranges of $4.5-15$Hz and $5-14$Hz which gives an overlapping frequency window of $5-14$Hz for Coh_{xy}. Therefore the peak occurring at 17Hz was discarded.

We adopted the above process in all conditions to verify whether there is a statistically significant coherence between

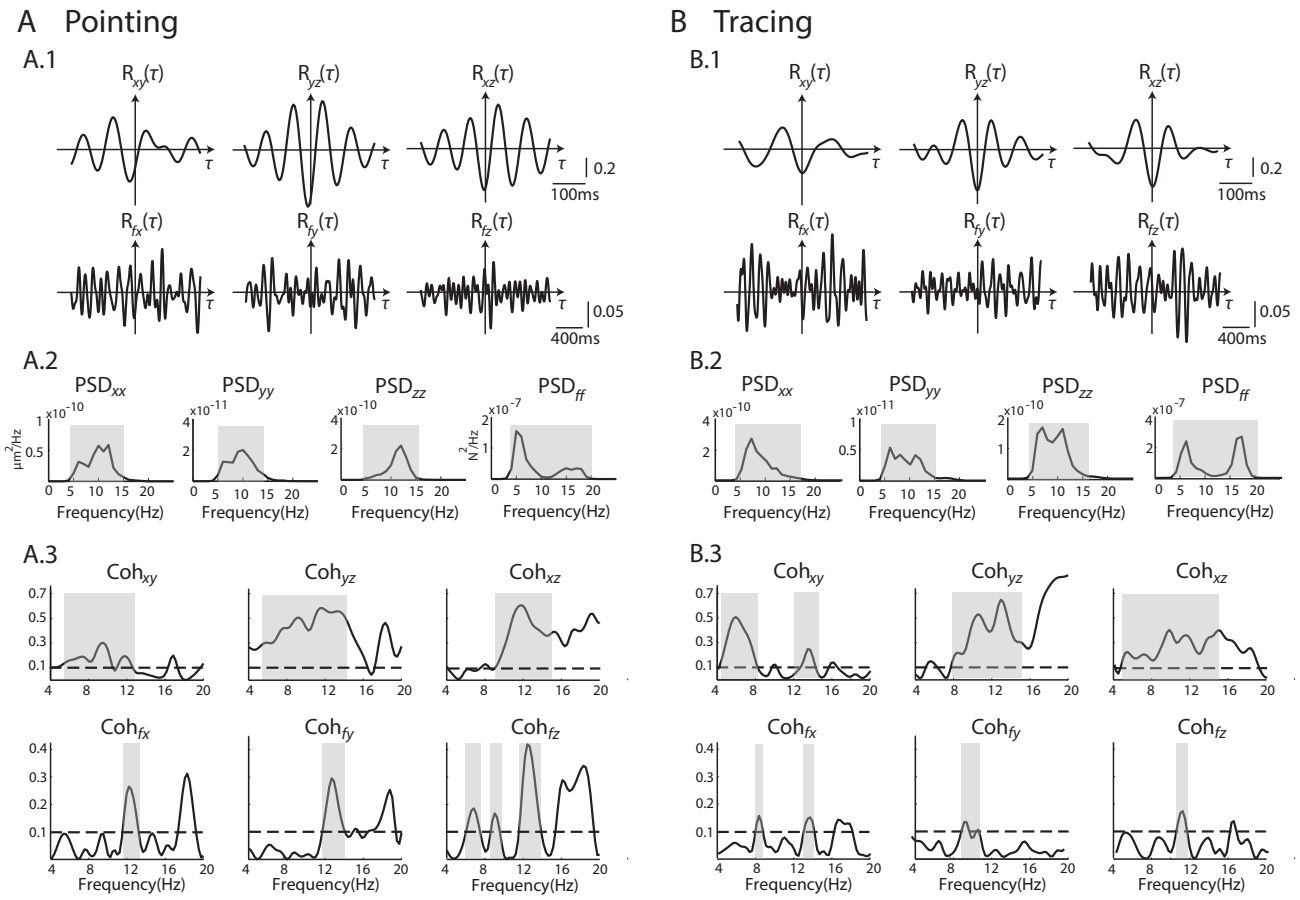

Fig. 4. Time- and frequency-domain correlation analysis in one representative surgeon subject in Pointing (A) and Tracing (B). A.1 and B.1 show the time-domain cross-correlation functions; A.2 and B.2 show the PSDs of the tremor in the *xyz* axes and the force *f* signal. Shaded area in A.3 and B.3 show the statistically significant coherence areas that were selected for further analysis.

the *xyz* and *f* data. We found moderate coherence between the tremor and force data which was subject- and task-dependent.

Lower plots in Figure 4 (A.3 and B.3) show coherence plots for the data from the same subject. This observation provided a strong evidence that the *xyz* tremor data are not independent and QwFLC-3D can lead to more accurate models. Moreover, the observed coherence between the tremor in the *xyz* axes and the grip force *f* motivated the test of QwFLC-4D. Supplementary Figure 1 depicts the same analysis for a representative novice subject.

B. QFLC Results - Synthetic Data

Figure 5A shows the modeling performance of QFLC and FLC for a representative segment of the simulated tremor data. QFLC showed better modeling of the tremor signal yielding smaller error than FLC. Figure 5B shows median RMSEs obtained from 10 iterations at each SNR value. The Figure 5B provides evidence of improved performance achieved with QFLC. Figure 5C shows that the time delay between the original and QFLC-modeled 10Hz signal reduces considerably faster than that between the original and FLC-modeled 10Hz signal.

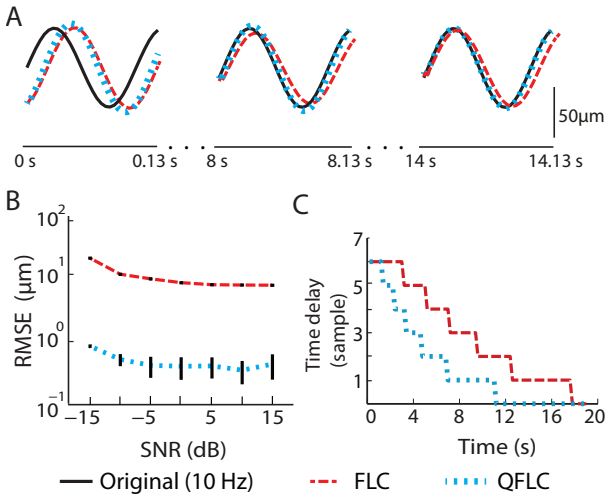

Fig. 5. (A) Modeling performance of the QFLC and FLC algorithms in tracking a simulated 10Hz sinusoidal signal, extracted with offline filtering of a modeled reaching task. (B) Median RMSEs at different SNRs with error bars representing variability (standard deviation) around the median. (C) Reduction in the time delay between the original and modeled sinusoidal signals due to adaptation.

C. QwFLC Results - Real Data

Figure 6 depicts a representative modeling performance in the same surgeon subject as in Figure 4. A close examination

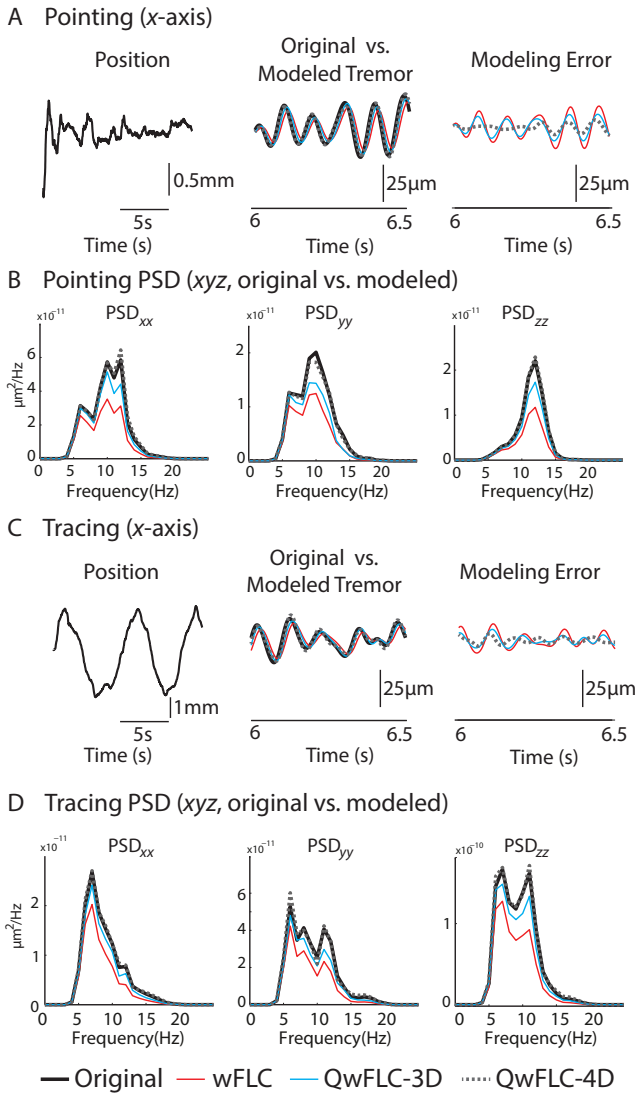

Fig. 6. QwFLC-4D outperforms both wFLC and QwFLC-3D. Results are shown in both tasks for the same subject as in Figure 4 and $\mu_{\mathcal{W}} = 0.075$ and $\mu_{\Omega} = 8 \times 10^{-5}$. (A) and (C) show the original position signals during pointing and tracing in the x-axis (left), the tremor and the modeled tremor with different algorithms (middle), and the modeling error (right). (B) and (D) show the spectrum of the original and modeled xyz tremor.

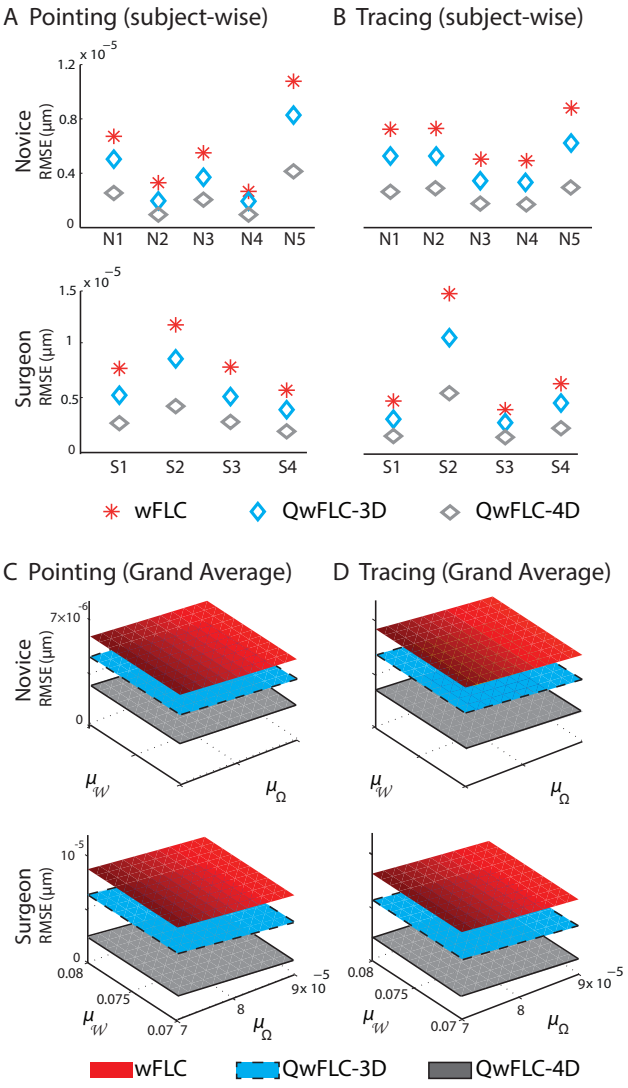

Fig. 7. QwFLC-4D outperforms both wFLC and QwFLC-3D in modeling tremor in terms of RMSE in both tasks. The lower the RMSE, better the modeling performance. (A) For individual novice subjects (B) For individual surgeons. In (A) and (B), results are shown when $\mu_{\mathcal{W}} = 0.075$ and $\mu_{\Omega} = 8 \times 10^{-5}$. (C) and (D) show average RMSE across subjects and across the x, y and z axes for different $\mu_{\mathcal{W}}$ and μ_{Ω} at intervals of 0.001 and 2×10^{-6}.

of the modeled tremor and modeling error in Figure 6A and C suggests that the QwFLC-4D outperforms both conventional wFLC and QwFLC-3D. Figure 6B and D show that QwFLC-4D can approximate the spectrum of the original tremor signal more accurately than wFLC and QwFLC-3D and the enhancement is across the whole tremor spectrum and not only in the frequencies in which the tremor in xyz and force signals were coherent, as was depicted in Figure 4.

Figure 7A, B show the RMSE yielded with wFLC, QwFLC-3D, and QwFLC-4D for each subject, averaged across xyz, in both pointing and tracing tasks for a special case of $\mu_{\mathcal{W}} = 0.075$ and $\mu_{\Omega} = 8 \times 10^{-5}$. For this special case, the average reduction in modeling error was 27% when using QwFLC-3D instead of 3 independent wFLCs. This average error reduced further by 40% when QwFLC-4D was used. Therefore, compared to wFLC, QwFLC-4D improved the modeling accuracy by 67% across all subjects, on average. Figure 7C,D show the average RMSE across all subjects and xyz for the different values of $\mu_{\mathcal{W}}$ and μ_{Ω}. Both variates of QwFLC outperformed the wFLC algorithm.

We then quantified the improvement in terms of the RMSE index versus the total area under the statistically significant coherence. Gray boxes in Figure 4 (A.3 and B.3) show an example of the included areas. In the top and the bottom subfigures of Figure 8, the total coherence area is calculated with $\mathrm{Coh}_{xy} + \mathrm{Coh}_{yz} + \mathrm{Coh}_{zx}$ and with $\mathrm{Coh}_{fx} + \mathrm{Coh}_{fy} + \mathrm{Coh}_{fz}$, respectively. We considered two cases: using QwFLC-3D instead of wFLC and using QwFLC-4D instead of QwFLC-3D. Linear regression was used to fit the data set from all 9 subjects in each fit. The top subfigures of Figure 8 show strong correlations ($R^2 = 0.63, p < 0.01$ and $R^2 = 0.78, p < 0.01$) between the improvement in RMSE (1D to 3D) and sum

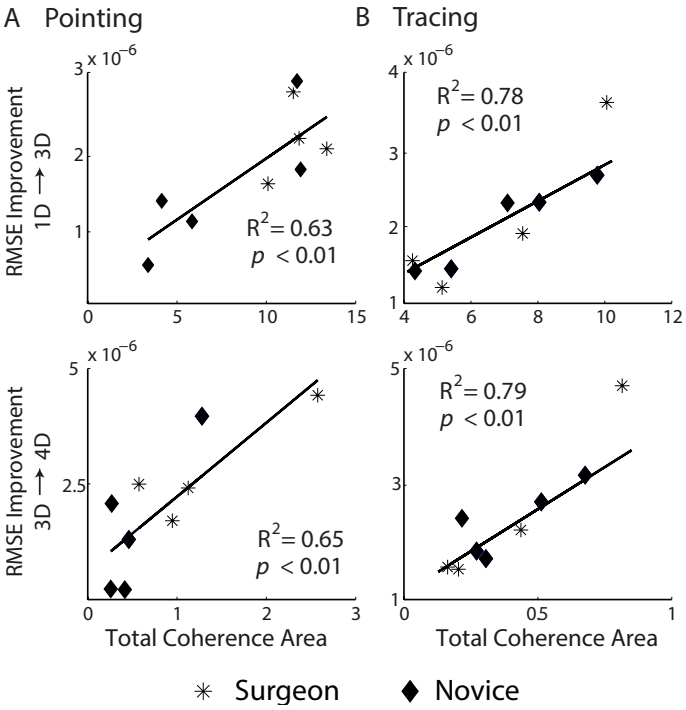

Fig. 8. Improvement in RMSE (1D to 3D and 3D to 4D)is proportional to the total coherence between xyz (top) and between xyz and f (bottom). Diamonds and stars represent novice and surgeon subjects, respectively. In all figures $\mu_W = 0.075$ and $\mu_\Omega = 8 \times 10^{-5}$.

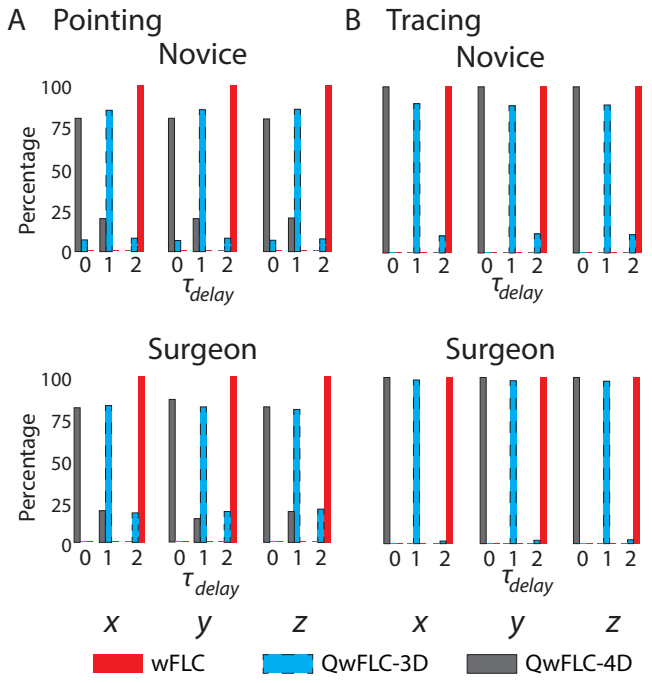

Fig. 9. Performance comparison between wFLC, QwFLC-3D, and QwFLC-4D in terms of the time delay between the original and the modeled signals. If a bar reaches 100% at $\tau_{delay} = x$, it shows that for all of the analysed 5s segments, the time lag between the original and modeled data was $x \times 4$ms.

coherence between xyz axes in the selected areas. Bottom subfigures show significant correlations ($R^2 = 0.65, p < 0.01$ and $R^2 = 0.79, p < 0.01$) between improvement in RMSE (3D to 4D) with total coherence between the xyz signals and f.

Moreover, we compared the performance of different algorithms in terms of the time delay of the peak cross-correlation function between the original and modeled signals. Figure 9 summarizes the percentage of the segments for which the time delay was 0, 1, or 2 lags (1 time lag is 4ms) for each algorithm. Between three algorithms, wFLC produced the slowest tracking performance with $\tau_{delay} = 2$ in 100% of the cases in both subject groups. This finding implies that the average time delay between the original and the wFLC-modeled tremor was on average 8ms. However the time lag between the original tremor and the modeled tremor with QwFLC-4D was 0 (that is, smaller than 4ms) for above 75% and above 95% of cases in the pointing and tracing tasks, respectively. The delay between the original and the estimated signals depends on the level of non-stationarity of the tremor signal and the adaptation delay. For the dataset that we analyzed the QwFLC-4D showed the fastest adaptation.

D. Computational Complexity

Real-time tremor compensation in robotics surgical instruments, requires the processes of tremor sensing and compensation to finish within a very short time, maximum 30ms [37]. Whether this time-delay can be considered appropriate in modern robotic microsurgery is understudied. wFLC can readily be implemented in real-time to compensate for the physiological tremor [13]. Table I presents a comparative study of computational complexity of FLC and wFLC versus QFLC and QwFLC. We have multiplied the complexity of FLC and wFLC by 3 to simulate parallel application in xyz. Using QwFLC, instead of 3 wFLC, increases the complexity linearly by 6 times ($82L$ vs. $27L/2$). Detailed derivation of computational complexity can be found in the Supplementary Material.

IV. Discussion

The use of robotic-assisted microsurgery is increasingly becoming wide-spread due to its robustness and high precision. Yet, removal of surgeon physiological tremor from the tip of the surgical device has remained a challenge. In this paper, we proposed a new class of algorithms based on quaternion algebra for modeling of tremor in 3-D and 4-D. Through time-domain correlation and coherence analysis we showed that the tremor data in different axes are not independent. We also demonstrated that there is significant coherence between the tremor data recorded in the xyz axes and the grip force f by which the surgeons hold or move the microsurgery tool. We showed that by taking into account such coupling information, the tremor modeling and the subsequent filtering performance can be improved significantly. We demonstrated that quaternion-based filtering is more accurate than the conventional one dimensional algorithms. We used an off-line zero-lag filter in our simulation. The linear filter used to extract the voluntary motion however would lead to up to $20ms$ delay in real-time application. This delay is within the range suggested by [37] but could degrade accuracy. Multi-step prediction is a potential approach to circumvent this problem [19], [35], [38]. QwFLC can be readily reformulated to achieve

TABLE I
COMPUTATIONAL COMPLEXITY OF DIFFERENT ALGORITHMS; THE FILTER ORDER IS DENOTED WITH L.

Algorithms	Additions	Multiplications	$O(.)$
3×LMS	$6L$	$6L+3$	$O(L)$
3×FLC	$6L$	$12L-3$	$O(L)$
3×wFLC	$3\times(3L+1)$	$3\times(9L+3)/2$	$O(L)$
QLMS [25]	$48L$	$56L$	$O(L)$
QFLC	$51L$	$64L-8$	$O(L)$
QwFLC	$67L+16$	$82L+14$	$O(L)$

tremor prediction. Preliminary results of combining multi-step prediction and QwFLC are presented in the Supplementary Material, Figures S2-4.

A. The source of oscillations in f

We showed that the coherence between the *xyz* tremor and f is statistically significant. However we did not draw any conclusions on the source of oscillations in f in the tremor frequency bands. In fact as early as 1956, Halliday and Redfearn [39] showed that at excessive force levels (up to 50N) (isometric contractions) the physiological tremor amplitude increases. This phenomenon was corroborated by others [40], [41]. However, to the best of the authors' knowledge, there is no evidence to support the oscillations in small forces (0-15N) that we observed are driven by a source in the neural system. There are therefore two competing hypotheses:

1) the oscillations recorded with the force sensor are generated by a source in the nervous system;
2) the oscillations recorded with the force sensor are the projection of the tremor in the *xyz* axes due to limb mechanics (possibly in combination with muscle dynamics).

Distinguishing between above two hypotheses will likely require recording of the electromyogram signals from both hand and wrist muscles in conjunction with the force and tremor [42]. This can quantify the synchrony between the tremor and motor unit firing and perhaps analysing these interactions at different hand posture or visual magnifications [43] is also required. However, from a practical point of view, including the force data in the QwFLC-4D algorithm improved modeling accuracy significantly comparing to the case of 3-D modeling with QwFLC-3D.

We did not find any significant difference between the surgeons and novice subjects tremor characteristics that would affect the QwFLC modelling. However, previously Veluvolu and Ang [36] showed that the fundamental characteristics of tremor is different between surgeon and novice subjects. For instance, they showed that surgeons' tremor exhibits more complex patterns and the bandwidth of surgeons' tremor signal is larger when compared to that in novice subjects.

B. Use of other quaternion adaptive filters

Circular (proper) signals are those with equal powers in all data axes and are mostly naturally occurring quaternions [44]. For instance, the hand physiological tremor is a circular 3-D signal with similar powers in *xyz*. Signals which are made complex by convenience of representation are often non-circular (improper) [25].

Recently variants of QLMS, such as the augmented QLMS (AQLMS) [25] and the widely-linear QLMS (WL-QLMS) [45], have been proposed to deal with non-circular signals.

AQLMS adopts the augmented statistics of the improper signals in modelling. However, the augmented statistics are inherent in QLMS [25] and hence QLMS and AQLMS will have similar performance for both circular and non-circular signals [25]. However, the computational complexity of AQLMS is almost twice larger than that of QLMS [25].

To cater for extra information from all correlation matrices of non-circular signals, WL-QLMS was proposed [44], [45]. Importantly, for circular signals WL-QLMS reduces to QLMS [44] and QLMS converges faster than WL-QLMS [45]. Hence for QwFLC-3D, QLMS is adequate and best suited.

In the 4D modeling condition, the grip force had higher power level compared to that on the *xyz* tremor signals. Therefore, to fully exploit correlation between axes, WL-QLMS could have been employed. However, to maintain consistency in performance comparison, we used QLMS in both 3D and 4D versions of QwFLC.

V. CONCLUSIONS

In current tremor modelling algorithm, data recorded in the *xyz* axes are analyzed independently. We showed that the *xyz* axes of tremor are not independent and the data in these axes feature significant subject- and task-dependent linear coupling. We also demonstrated that there is a considerable level of coherence between the data recorded in the *xyz* axes and the grip force by which the device is held or moved. In order to exploit the mutual coupling information between *xyz* tremor axes and force we proposed a new class of algorithms based on quaternion algebra for modeling of tremor in 3-D and 4-D. Taking into account the coupling between the data in the *xyz* axes and the force data, the error in tremor modeling reduced by 67%. The QwFLC algorithm can be implemented in real-time because it is only 6 times more complex than 3 parallel wFLC blocks.

VI. APPENDIX

A. Quaternions: Basic Algebra

Quaternion dimensions are defined by three orthogonal standard basis vectors i, j and k and $ijk = i^2 = j^2 = k^2 = -1$. The unit vectors are non-commutative; for instance $i = jk = -kj$. A quaternion variable $Q(Q_a, Q_{b,c,d})$ is an augmented form of a complex number and can be written as

$$Q = Q_a + Q_b i + Q_c j + Q_d k$$

where the scalar (real) component is denoted by Q_a and the imaginary parts are Q_b, Q_c and Q_d. Addition of two quaternions Q_1 and Q_2 is a quaternion with

$$\begin{aligned} Q_a &= Q_{1,a} + Q_{2,a} \\ Q_{b,c,d} &= (Q_{1,b} + Q_{2,b})i + (Q_{1,c} + Q_{2,c})j + (Q_{1,d} + Q_{2,d})k. \end{aligned}$$

Multiplication of two quaternions is non-commutative ($Q_1Q_2 = -Q_2Q_1$) and is given by

$$\begin{aligned} Q_1Q_2 &= (Q_{1,a} + Q_{1,b,c,d})(Q_{2,a} + Q_{2,b,c,d}) \\ &= Q_{1,a}Q_{2,a} - Q_{1,b,c,d} \cdot Q_{2,b,c,d} + Q_{2,a}Q_{1,b,c,d} \\ &+ Q_{1,a}Q_{2,b,c,d} + Q_{1,b,c,d} \times Q_{2,b,c,d}. \end{aligned}$$

Finally, Q^*, the conjugate of Q, is $(Q_a, -Q_{b,c,d})$.

References

[1] A. Anouti and W. C. Koller, "Tremor disoders: diagnosis and management," *The Western J. Med.*, vol. 162, no. 6, pp. 510–513, 1992.

[2] J. H. McAuley and C. D. Marsden, "Physiological and pathological tremors and rhythmic central motor control," *Brain*, vol. 123, pp. 1545–1567, 2000.

[3] C. N. Riviere and N. V. Thakor, "Modeling and canceling tremor in human-machine interfaces," *IEEE Eng. Med. Biol. Mag.*, vol. 56, no. 3, pp. 29–36, 1996.

[4] W. T. Ang, P. K. Khosla, and C. N. Riviere, "Design of all-accelerometer inertial measurement unit for tremor sensing in hand-held microsurgical instrument," *IEEE Int. Conf. Robo. Auto.*, vol. 2, pp. 1781–1786, 2003.

[5] K. C. Veluvolu, W. T. Latt, and W. T. Ang, "Double adaptive bandlimited multiple Fourier linear combiner for real-time estimation/filtering of physiological tremor," *Biomed. Sig. Process. Cont.*, vol. 5, no. 1, pp. 37–44, 2010.

[6] K. C. Veluvolu and W. T. Ang, "Estimation of physiological tremor from accelerometers for real-time applications," *Sensors*, vol. 11, no. 3, pp. 3020–3036, 2011.

[7] S. Tatinati, K. C. Veluvolu, S. Hong, W. T. Latt, and W. T. Ang, "Real-time tremor modeling with auto-regressive model and Kalman filter for surgical robotics applications," *IEEE Sens. J.*, vol. 13, no. 12, pp. 4977–4985, 2013.

[8] W. Reynolds, "The first laparoscopic cholecystectomy," *J. Soc. Laparoendoscopic Surgeons*, vol. 5, pp. 89–94, 2001.

[9] R. H. Taylor, J. Funda, B. Eldridge, S. Gomory, K. Gruben, D. LaRose, M. Talamini, L. Kavoussi, and J. Anderson, "A telerobotic assistant for laparoscopic surgery," *IEEE Eng. Med. Biol. Mag.*, vol. 14, no. 3, pp. 279–288, 1995.

[10] C. Bergeles and G.-Z. Yang, "From passive tool holders to microsurgeons: safer, smaller, smarter surgical robots," *IEEE Trans. Biomed. Eng.*, vol. 61, no. 5, pp. 1565–76, 2014.

[11] V. Ficarra, S. Cavalleri, G. Novara, M. Aragona, and W. Artibani, "Evidence from robot-assisted laparoscopic radical prostatectomy: A systematic review," *European Urology*, vol. 51, no. 1, pp. 45–56, 2007.

[12] R. Taylor, "A steady-hand robotic system for microsurgical augmentation," *Int. J. Robot. Res.*, vol. 18, no. 12, pp. 1201–1210, 1999.

[13] C. N. Riviere, W. T. Ang, and K. P. Khosla, "Toward active tremor canceling in handheld microsurgical instruments," *IEEE Trans. Robot. Autom.*, vol. 19, no. 5, pp. 793–800, 2003.

[14] B. Gonenc, J. Handa, P. Gehlbach, R. H. Taylor, and I. Iordachita, "A Comparative Study for Robot Assisted Vitreoretinal Surgery: Micron vs. the Steady-Hand Robot.," *2013 IEEE International Conference on Robotics and Automation*, pp. 4832–4837, 2013.

[15] C. N. Riviere, R. S. Rader, and N. V. Thakor, "Adaptive cancelling of physiological tremor for improved precision in microsurgery," *IEEE Trans. Biomed. Eng.*, vol. 45, no. 7, pp. 839–46, 1998.

[16] T. H. Hall, F. de Carvalho, and A. Jackson, "A common structure underlies low-frequency cortical dynamics in movement, sleep, and sedation," *Neuron*, vol. 83, no. 5, pp. 1185–1199, 2014.

[17] T. M. Hall, K. Nazarpour, and A. Jackson, "Real-time estimation and biofeedback of single-neuron firing rates using local field potentials," *Nature Communications*, vol. 5, p. 5462, 2014.

[18] A. V. Oppenheim and R. W. Schaefer, *Discrete-Time Signal Processing*. Prentice-Hall, Bergen Country, NJ, USA, 2001.

[19] J. A. Gallego, E. Rocon, J. O. Roa, J. C. Moreno, and J. L. Pons, "Real-time estimation of pathological tremor parameters from gyroscope data," *Sensors*, vol. 10, no. 3, pp. 2129–2149, 2010.

[20] C. Vaz, X. Kong, and N. V. Thakor, "An adaptive estimation of periodic signals using a Fourier linear combiner," *IEEE Trans. Sig. Process.*, vol. 42, no. 1, pp. 1–10, 1994.

[21] V. Bonnet, C. Mazzà, J. McCamley, and A. Cappozzo, "Use of weighted Fourier linear combiner filters to estimate lower trunk 3D orientation from gyroscope sensors data," *J. Neuroeng Rehabil.*, vol. 10, no. 9, 2013.

[22] L. Z. Popović, T. B. Sekara, and M. B. Popović, "Adaptive band-pass filter (ABPF) for tremor extraction from inertial sensor data," *Comp. Meth. Prog. Biomed.*, vol. 99, no. 3, pp. 298–305, 2010.

[23] B. Chen, Q. Liu, X. Sun, X. Li, and H. Shu, "Removing Gaussian noise for colour images by quaternion representation and optimisation of weights in non-local means filter," *IET Sig. Process.*, vol. 8, no. 10, pp. 591–600, 2014.

[24] C. Cheong Took, G. Strbac, K. Aihara, and D. P. Mandic, "Quaternion-valued short term joint forecasting of three-dimensional wind and atmospheric parameters," *Renew. Energy*, vol. 36, no. 6, pp. 1754–1760, 2011.

[25] C. Cheong Took and D. P. Mandic, "The quaternion LMS algorithm for adaptive filtering of hypercomplex processes," *IEEE Trans. Sig. Process.*, vol. 57, no. 4, pp. 1316–1327, 2009.

[26] K. Adhikari, S. Tatinati, K. C. Veluvolu, and K. Nazarpour, "Modeling 3d tremor signals with a quaternion weighted Fourier linear combiner," in *Neural Engineering (NER), 7th Int IEEE/EMBS Conf*, pp. 799–802, April 2015.

[27] K. Adhikari, S. Tatinati, K. C. Veluvolu, and K. Nazarpour, "Improvement in modelling of physiological tremor by inclusion of grip force in quaternion weighted fourier linear combiner," in *in Proc. IET Intelligent Signal Processing Conference, 2nd IET ISP Conf*, December 2015.

[28] E. L. Su, W. T. Latt, W. T. Ang, T. C. Lim, C. L. Teo, and E. Burdet, "Micromanipulation accuracy in pointing and tracing investigated with a contact-free measurement system," in *Eng. Med. Biol. Conf., Int IEEE/EMBS (EMBC)*, pp. 3960–3963, 2009.

[29] T. L. Win, U. X. Tan, C. Y. Shee, and W. T. Ang, "Design and calibration of an optical micro motion sensing system for micromanipulation tasks," in *Robot. Autom., IEEE Int. Conf.*, pp. 3383–3388, April 2007.

[30] T. L. Win, U. X. Tan, K. C. Veluvolu, J. K. D. Lin, C. Y. Shee, and W. T. Ang, "System to assess accuracy of micromanipulation," in *Eng. Med. Biol. Conf., Int IEEE/EMBS (EMBC)*, pp. 5744–5747, 2007.

[31] J. R. Rosenberg, A. M. Amjad, P. Breeze, D. R. Brillinger, and D. M. Halliday, "The Fourier approach to the identification of functional coupling between neuronal spike trains," *Prog. Biophysics Molecu. Biol.*, vol. 53, no. 1, pp. 1–31, 1989.

[32] A. M. Amjad, D. M. Halliday, J. R. Rosenberg, and B. A. Conway, "An extended difference of coherence test for comparing and combining several independent coherence estimates: Theory and application to the study of motor units and physiological tremor," *J. Neurosci. Meth.*, vol. 73, pp. 69–79, 1997.

[33] D. M. Halliday, J. R. Rosenberg, A. M. Amjad, P. Breeze, B. A. Conway, and S. F. Farmer, "A framework for the analysis of mixed time series/point process data–theory and application to the study of physiological tremor, single motor unit discharges and electromyograms," *Prog. Biophys. Mol. Biol.*, vol. 64, no. 2-3, pp. 237–278, 1995.

[34] K. Nazarpour, A. Barnard, and A. Jackson, "Flexible cortical control of task-specific muscle synergies," *J. Neurosci.*, vol. 32, no. 36, pp. 12349–12360, 2012.

[35] S. Tatinati, K. Veluvolu, and W. T. Ang, "Multistep prediction of physiological tremor based on machine learning for robotics assisted microsurgery," *IEEE Trans. Cybernetics*, vol. 45, no. 2, pp. 328–339, 2015.

[36] K. Veluvolu and W. T. Ang, "Estimation and filtering of physiological tremor for real-time compensation in surgical robotics applications," *Int. J. Med. Robot.*, vol. 6, no. 3, pp. 334–342, 2010.

[37] H. N. Jacobus, A. J. Riggis, C. J. Jacobus, and Y. Weinstein, "Implementation issues for telerobotic handcontrollers: Human-robot ergonomics," in *Human Robot Interaction* (M. Rahimi and W. Karwowski, eds.), pp. 284–314, Taylor & Francis, 1992.

[38] K. C. Veluvolu, S. Tatinati, S. Hong, and W. T. Ang, "Multi-step prediction of physiological tremor for surgical robotics applications," *IEEE Trans. Biomed. Eng.*, vol. 60, no. 11, pp. 3074–3082, 2013.

[39] A. M. Halliday and J. W. T. Redfearn, "An analysis of frequencies of finger tremor in healthy subjects," *J. Physiol. Lond.*, vol. 134, no. 3, pp. 600–611, 1956.

[40] G. G. Sutton and K. Skykes, "The variation in hand tremor with force in healthy subjects," *J. Physiol. Lond.*, vol. 191, no. 3, pp. 699–711, 1967.

[41] G. C. Joyce and P. M. H. Rack, "The effects of load and force on tremor at the normal human elbow joint," *J. Physiol. Lond.*, vol. 240, no. 2, pp. 375–396, 1974.

[42] C. N. Christakos, N. A. Papadimitriou, and S. Erimaki, "Parallel neuronal mechanisms underlying physiological force tremor in steady muscle contractions of humans," *J. Neurophysiol.*, vol. 95, no. 1, pp. 53–66, 2006.

[43] B. Safwat, E. L. Su, R. Gassert, C. L. Teo, and E. Burdet, "The role of posture, magnification, and grip force on microscopic accuracy," *Ann. Biomed. Eng.*, vol. 35, no. 5, pp. 997–1006, 2009.
[44] C. Cheong Took, C. Jahanchahi, and D. P. Mandic, "A unifying framework for the analysis of quaternion valued adaptive filters," in *Asilomar Conf Sig. Sys. Comp.*, pp. 1771–1774, 2011.
[45] C. Cheong Took and D. P. Mandic, "A quaternion widely linear adaptive filter," *IEEE Trans. Sig. Process.*, vol. 58, no. 8, pp. 4427–4431, 2010.

Kabita Adhikari (S'14) received her B.E. in Electronics and Communication Engineering from Institute of Engineering, Tribhuvan University, Nepal in 2004. She received her MSc degree in Optoelectronics and Communication Systems in 2007 from Northumbria University, UK. From 2008 to 2010 she worked as a lecturer in South Tyneside College. She then joined Newcastle University in 2010 as a Teaching Fellow.

Currently along with her academic role, she reads for a Ph.D. degree at Newcastle University, UK. Her Research interests include biomedical signal processing and adaptive filtering.

Sivanagaraja Tatinati (S'13) received the B.Tech. degree in electronics and communication engineering from Acharya Nagarjuna University, Guntur, India, in 2010, and the Ph.D. degree in school of electronics engineering at Kyungpook National University, South Korea in 2015.

His current research interests include robotics assisted medical instruments, adaptive filtering, machine learning techniques based regression, application of estimation and prediction algorithms in biomedical engineering.

Wei Tech Ang (S'98-M'04) received the B.E. and M.E. degrees in mechanical and production engineering from Nanyang Technological University, Singapore, in 1997 and 1999, respectively, and the Ph.D. degree in robotics from Carnegie Mellon University, Pittsburgh, PA, USA, in 2004.

Since 2004, he has been with the School of Mechanical and Aerospace Engineering, Nanyang Technological University, where he is currently an Associate Professor and holds the appointment of Head of Engineering Mechanics Division. His research focuses on robotics technology for Biomedical applications, which include surgery, rehabilitation and cell micromanipulation.

Kalyana C. Veluvolu (S'03-M'06-SM'13) received the B.Tech. degree in electrical and electronic engineering from Acharya Nagarjuna University, Guntur, India, in 2002, and the Ph.D. degree in electrical engineering from Nanyang Technological University, Singapore, in 2006.

During 20062009, he was a Research Fellow with the Biorobotics Group, Robotics Research Center, Nanyang Technological University. Since 2009, he has been with the School of Electronics Engineering, Kyungpook National University, Daegu, Korea, where he is currently an Associate Professor. He has been a Principal Investigator or a Co-investigator on a number of research grants funded by the National Research Foundation of Korea, and other agencies. He has authored or co-authored over 100 journal articles and conference proceedings. His current research interests include nonlinear estimation and filtering, braincomputer interface, biomedical signal processing, and surgical robotics.

Kianoush Nazarpour (S'05-M'08-SM'14) received the B.Sc. degree from KN Toosi University of Technology, Tehran, Iran, in 2003, the M.Sc. degree from Tarbiat Modarres University, Tehran, Iran, in 2005, and the Ph.D. degree from Cardiff University, Cardiff, U.K., in 2008 all in Electrical and Electronic Engineering. From 2007 to 2012, he held two post-doctoral researcher posts at Birmingham and Newcastle universities. During Summer 2009, he was a visiting scholar at Northwestern and Columbia universities, USA. In 2012, he joined Touch Bionics Inc., U.K. as a Senior Algorithm Engineering working on intelligent control of multi-functional myoelectric prostheses. Dr Nazarpour returned to Newcastle University as a Lecturer in Biomedical Engineering in 2013. His research interests include intelligent sensing and biomedical signal processing and their applications in assistive technology.

Dr Nazarpour received the Best Paper award in the 3rd International Brain-Computer Interface (BCI) Conference (Graz, 2006), and the David Douglas award (2006), U.K., for his work on joint space-time-frequency analysis of the electroencephalogram signals. Dr Nazarpour is currently an Associate Editor for the Medical Engineering and Physics journal in the area of Biomedical Signal Processing.